Aerodynamical sticking of dust aggregates

Gerhard Wurm*
Laboratory for Atmospheric and Space Physics, University of Colorado at Boulder, Campus Box 392, Boulder, Colorado 80309-0392

Jürgen Blum
Astrophysical Institute and University-Observatory, Friedrich-Schiller-Universtität Jena, Schillergässchen 2, 07745 Jena, Germany

Joshua E. Colwell
Laboratory for Atmospheric and Space Physics, University of Colorado at Boulder, Campus Box 392, Boulder, Colorado 80309-0392
(Received 3 April 2001; published 21 September 2001)

We present results of collision experiments of a dense beam of aggregated 1.2 μm SiO_2 particles entrained in a gas flow with metal targets of different widths. Depending on the target width ($d=25.4$, 50.8, and 127 μm) and the ambient gas pressure ($p=0.5$–2.0 mbar), the growth of a dust pile on the target begins at a threshold impact speed ($v_{imp}=6$–12.5 m/s). These threshold velocities for sticking exceed the limit for total disruption of aggregates by more than a factor of 5–10 for the given parameters. We found that a significant number of fragments (single particles) from the collisions had a very low coefficient of restitution c_r at least down to $c_r<0.05$ that is much lower than the value $c_r>0.5$ that one of the single solid micron-sized particles would have while impinging a rigid target. Due to the drag of the gas flow these slow fragments are forced back to the target a second time resulting in sticking that eventually leads to the formation of the dust pile in spite of the high impact velocities. Together, the fragmentation, the low coefficients of restitution of a significant number of fragments, and the gas flow provide an efficient growth mechanism for bodies that would otherwise lose mass. We consider this an important mechanism for the formation of planetesimals in the solar nebula.

DOI: 10.1103/PhysRevE.64.046301 PACS number(s): 61.43.Hv, 81.05.Rm, 83.50.−v, 96.10.+i

I. INTRODUCTION

The main motivation for the work presented here originates in the attempt to understand the early phases of planet formation in more detail. However, the basic concept behind this research is of general importance. It may have applications in all branches where dust powders are handled and where their sticking properties are essential. With this in mind we will continue to outline the problems of planet formation assuming that the same ideas might be used apart from astrophysics.

It is widely accepted that planet formation starts with (sub)micron-sized dust particles in a gas-dust disk that grow to kilometer-sized bodies due to inelastic mutual collisions and attractive surface forces. The gas in the disk exerts different drag forces on the dust. The particles therefore get different velocities and collide, stick together, and grow to kilometer-sized planetesimals. However, only fractions of this growth over several orders of magnitude in size are understood so far. In the first stages micron-sized particles grow to centimeter-sized bodies, and sticking and growth has actually been observed in laboratory experiments [1,2]. On the other hand all the following stages remain more enigmatic. In particular, due to maximal radial drift velocities [3], meter-sized bodies have such short lifetimes that their growth rate must be enormously fast to allow for the formation of larger planetesimals. It is a growth mechanism for those later stages of centimeter- to kilometer-sized bodies that might be revealed in the light of our experiments.

In recent years some (but few) experiments showed that effective growth of micron-sized particles is possible. It turned out in previous experiments by Poppe *et al.* [4] with spherical 1.2 μm (diameter) amorphous SiO_2 particles that a critical sticking velocity of $v_c=1.1$–1.3 m/s could be defined. Particles with impact speeds $v_{imp}<v_c$ impinging on a rigid target will stick due to sufficient energy loss and binding surface forces. Thus, as long as the collision velocities are below a given threshold velocity, an effective growth of larger structures takes place. Particles with higher impact velocities, however, bounce off. Rebounds are described by a coefficient of restitution c_r defined as

$$c_r=v_{reb}/v_{imp}. \tag{1}$$

Here, v_{imp} is the impact speed and v_{reb} is the rebound speed. Poppe *et al.* [4] found coefficients of restitution as high as $c_r\approx0.8$, above (but close to) the critical velocity and decreasing to $c_r\approx0.5$ for $v_{imp}\approx15$ m/s. A different kind of experiment by Wurm and Blum [1] showed that for very low collision velocities the self-consistent growth of dust in a dust cloud is a cluster-cluster type process (cluster-cluster aggregation or CCA). Here, aggregates of similar size collide and form fluffy (fractal) structures (up to $r\approx100$ μm in size in the experiments cited). Yet another set of experiments by Blum and Wurm [2] showed that such aggregates are disrupted if the collision velocity lies above $v_{imp}\approx2.6$–3.5 m/s for 1.2 μm SiO_2 particle aggregates and above $v_{imp}\approx1.2$–1.9 m/s for 1.9 μm SiO_2 particle aggre-

*FAX (+001) 303 492 6946.
Email address: gerhard.wurm@lasp.colorado.edu

gates. Calculations using the model by Dominik and Tielens [5] but including the experimental values for the critical sticking velocity by Poppe *et al.* [4] and the rolling-friction force by Heim *et al.* [6] are in excellent agreement with the experimental results for the 1.9 μm SiO_2 particles [2] but predict disruption even at lower impact velocities for the 1.2 μm SiO_2 particle aggregates. Probably the value measured by Blum and Wurm [2] for these smaller monomers is already biased by the effect that we will present here. Another result comes from an earlier experimental study by Blum and Münch [7] of millimeter-sized aggregate-aggregate collisions at cm/s to m/s collision velocities. Only restitution and fragmentation could be observed. Finally, experiments by Supulver *et al.* [8] show that even with the assumption of a very sticky frost layer covering larger (centimeter-sized) bodies only very small collision velocities (<1 cm/s) can result in sticking. The conclusion from all the results mentioned above is that, to date, there has been no experimental evidence why larger bodies in protoplanetary disks should be formed at all, but are not shattered to pieces again, once they reach sizes of approximately 0.1 m.

To offer a solution to this major problem in planet formation, it is crucial to note that all these findings apply to a system where collisions are ballistic. This means that gas is often supposed to generate relative velocities but should be of no importance for the outcome of a collision itself. This condition is not always fulfilled, particularly if compound bodies collide. Such bodies collide quite differently from rigid bodies. They can fragment with a distribution of coefficients of restitution that can reach very low values rather than rebounding with a single high value $c_r > 0.5$. Though the impactor is solid and the target is a dust layer, experiments by Colwell and Taylor [9] already support this view. Energy is distributed in different ways if collisions are not between two rigid bodies, because coefficients of restitution have been measured to be relatively low down to $c_r < 0.03$ in their experiments. In the case of very low coefficients of restitution of a significant number of fragments from a collision of an aggregated particle, gas drag cannot be neglected. It might be strong enough to change the path of particles already in the vicinity of the collision point. This can result in further low velocity collisions that will lead to sticking due to the new reduced impact velocity. This mechanism has already been suggested by Wurm [10]. The experiments described here are the first systematic approach to the problem, and first results are given in Wurm *et al.* [11]. Here we describe the experiment in more detail and give a first quantitative model describing the results of the experiments.

To study the collisions of an aggregate embedded in a gas flow we directed an entrained beam of aggregates on targets of varying widths and at different ambient pressures. As a quantitative measure to describe collisions under the influence of a gas flow in this paper we define the scale parameter S as

$$S = \frac{\lambda}{d}, \tag{2}$$

where λ is the mean free path length of the gas molecules and d denotes the width of a metal foil used (edge on) as a target. If the other target dimension were not effectively infinite and d were an overall characteristic size of the target the scale parameter S would then equal the Knudsen number. This is usually used to describe different regimes of particle-gas interaction. We suggest viewing both parameters as similar, since the effects described below are most probably not influenced much by the virtually infinite extension of the target in the second dimension. The results reported here describe scale parameters in the range of $S = 0.3$–4. As far as protoplanetary disks are concerned, mean free pathlengths of the gas molecules in the midplane might be as short as a few millimeter going up to several meter from 1 AU (Astronomical Unit) to 10 AU, respectively [12]. Impacts are supposed to fragment bodies of several centimeter in size because they occur at $v > v_c$ with v being several m/s. Hence, in terms of the scale parameter, the experimental settings match the conditions in those disks for the stages when fragmentation is supposed to get important. An increased threshold velocity for sticking for those bodies would allow a net growth of the larger body due to the collection of fragments. This provides an efficient process for growth and might explain growth where ballistic models suggest fragmentation or destruction of preplanetary objects.

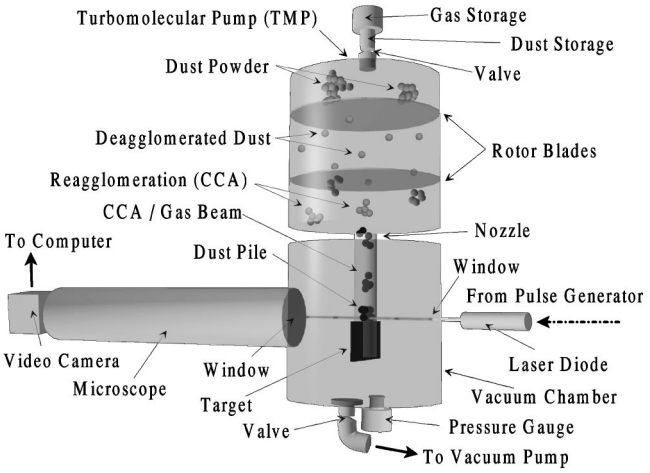

FIG. 1. Schematics of the experiment.

II. EXPERIMENTAL APPROACH

The general setup of the experiment is shown in Fig. 1. The basic component is a particle aggregate beam generator based on a turbomolecular pump (TMP) described in Wurm and Blum [1], Blum *et al.* [13], and Blum and Wurm [2]. It produces a beam of CCA clusters. With the given experimental parameters, the mean aggregate consists of approximately ten single particles. The aggregates are embedded in a thin gas. The pressure ranges from approximately $p = 0.5$ mbar to $p = 2$ mbar in the experiments. Corresponding mean free pathlengths for the gas molecules in the given pressure range are $\lambda = 132$ μm down to $\lambda = 33.5$ μm, respectively. The pressure is measured at a time of the experiment when the pressure inside the vacuum chamber is essentially balanced, which is achieved fraction of a second after the injection

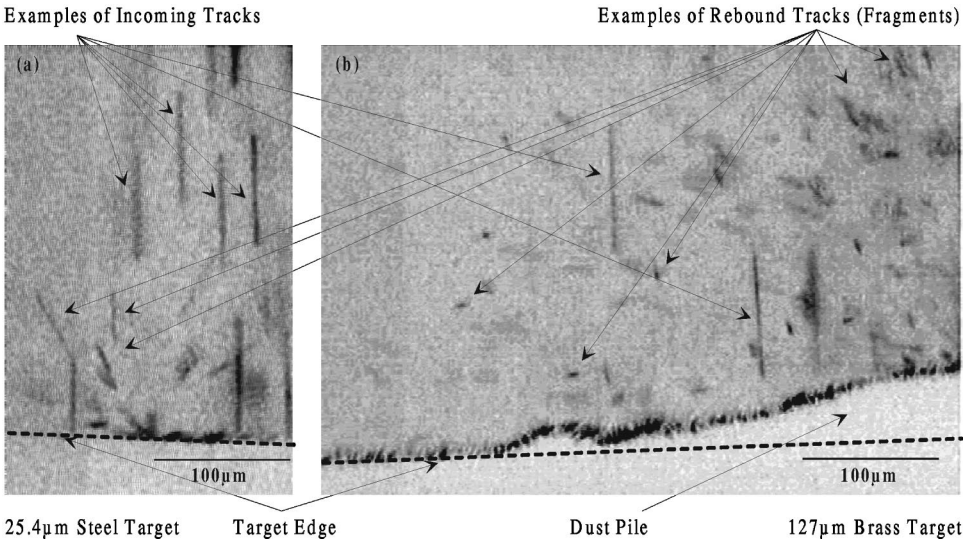

FIG. 2. Examples of particle tracks and target edge imaging.

starts. We estimate the readout error for the pressure to be less than 10%. Upon the time of dust and gas injection the grains leaving the TMP have initial velocities up to 30 m/s decreasing to sedimentation velocities of a few cm/s in approximately 5 s. The particle beam width is of the order of 100 μm in radius. The grain-gas beam is directed to the edge of a foil of thickness (width) d supported inside a vacuum chamber. Target thicknesses are $d=25.4,\ 50.8$, and 127 μm. The grains hit the edge of the target perpendicularly. A microscope is focused on the target edge where the target intersects the particle beam. Both the particle beam and the target edge are in the focal plane of the microscope. The field of view is illuminated by a pulsed laser beam. By slightly oblique illumination only scattered light is detected resulting in a sufficient contrast of bright imaged particles on a dark background. The images are taken with a video camera at 25 frames per second and directly digitized to a computer.

Presented as two examples in Fig. 2 the images show the edge of the target, i.e., the metal target itself or the uppermost layer of particles on the target. In addition, they show particle tracks of incoming and bouncing particles. The lengths of the tracks are determined by the velocity of the particles and the pulse length of the laser beam and therefore give a measure of the velocities. At a given time all particles in the beam have the same velocity, which together with errors in the determination of the track lengths has an uncertainty of approximately 5%. At a given time, when the beam velocity decreases below a certain value, a layer of particles forms on the target growing continuously at lower velocities. We analyze the images before and after the onset of growth and determine the corresponding impact speeds v_{imp} of the aggregates, respectively. This gives an uncertainty interval for the threshold velocity v_{stick} at the onset of growth. The particle beam is subject to minor random changes in intensity, and, especially at higher pressures, velocities decrease rapidly between consecutive images. Also, the beam might slightly alter its intersection area with the target at the given small sizes. Due to these variations, the beginning of growth could not always be identified unambiguously on two subsequent images. The uncertainty interval in those cases is rather large and no additional confining information can be gained apart from the data shown later. Within their large error bars they are consistent with the other data, but due to the lack of new information are not shown otherwise. As the main result we obtain the threshold velocity of sticking v_{stick} as a function of the target scale parameter S. This is shown in Fig. 3 where the data are adapted from Wurm *et al.* [11]. Throughout the experiments a dust sample consisting of

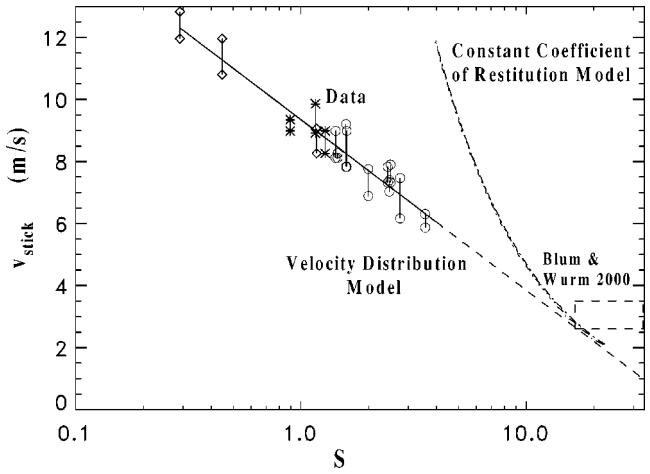

FIG. 3. Dependence of the threshold velocity for sticking, v_{stick}, on the scale parameter S, which depends on the gas pressure and the target thickness. Diamonds: 127 μm brass target; asterisks: 50.8 μm brass target; circles: 25.4 μm steel target. The variation in data points belonging to a given target was accomplished by changing the pressure. Upper and lower values for a given data point are the velocities before and after the onset of growth on the target. The dashed box in the lower right corner indicates a value from Blum and Wurm [2]. The data are described by the velocity distribution model (solid line) and is extrapolated beyond the data as dashed line (see text for details). The dashed-dotted curves describe a constant coefficient of restitution model ($c_r=0.3$, rebound angle $\alpha=45°$). The two almost identical curves only differ in the actual choice of pressure of 2 mbar and 0.2 mbar (refer to text for details).

1.2 μm diameter amorphous SiO_2 (glass) spheres is used. The data are consistent with a simple logarithmic dependence fitted as solid line to the data. Extrapolating, this would also be in agreement with earlier experimental results by Blum and Wurm [2] at very small target thickness and low pressure indicated by the dashed box in the lower right corner. The targets were commercial steel and brass foils and the edges were not treated in any additional special way. This means that a certain roughness might be present on the edges. However, the result obviously did neither depend on the material as far as the two samples are concerned (or three, including the Si_3N_4 cantilever referring to the dashed box) nor on a perfect flat edge.

As an additional feature of the beam generator, small aggregates can be produced during the initial preparation of the experiment when a vacuum pump is evacuating the chamber. These are embedded in a gas flow of much lower pressure and have a more or less stable velocity over several seconds. In agreement with the data shown in Fig. 3, the velocities at the corresponding scale parameters for the small and intermediate target size were above the threshold velocity for sticking, and therefore no sticking but only fragmentation could be observed. On the other hand, a slow growth of a dust pile could be observed for the large target size. The particle velocity obviously exactly matched the threshold velocity. This data point is included in Fig. 3 as the third and lowest value ($S=1.18, v_{stick}=8.66$ m/s) for the 127 μm target and is consistent with the other data.

III. DISCUSSION

The data show a clear dependence of the sticking velocity on the scale parameter. This can be explained by means of two main facts:

• At the given velocities, CCA aggregates totally fragment into their single components. This has been shown before [2,5]. However, a significant part of the fragments (the single particles that constitute the aggregate) in an aggregate collision will rebound from the target with much lower velocities than a single impacting particle would. This is because a significant amount of the impact energy is dissipated by breaking up the aggregate and ejecting particles from the target. There is a broad distribution of fragment energies and rebound angles.

• The aggregates colliding with the target are almost perfectly coupled to the gas, because the gas-grain friction times are very small [a few milliseconds as calculated by Eq. (4)]. Therefore the gas velocity and the dust particle velocity in the beam are equal. As soon as the fragments rebound from the target they feel this gas flow as a decelerating head wind, which causes them to change direction. Depending on their speeds and rebound angles this brings them into contact with the target a second time where, this time, they can stick due to their low velocities.

The given data do not allow us to measure a precise distribution of energy or velocities of the rebounding particles in the case where the dust piles are forming. The reagglomeration is a rather rapid process and only a few images are available for each experiment before the whole field of view is filled with an opaque dust pile. However, as can readily be seen by measuring the tracks of incoming and rebounding particles in Fig. 2(b), velocities certainly range down to only a few percent of the collision velocity, far below values for single particle impacts without fragmentation. With this in mind we calculated the trajectories of rebound particles. The force F acting on a particle in the given rarefied gas flows can be described by

$$F=\frac{m}{\tau_f}v_{gas}, \tag{3}$$

where m is the particle mass, τ_f is the gas-grain friction time, and v_{gas} is the gas velocity with respect to the particle. The gas-grain friction time can be calculated using Eq. (20) in Blum *et al.* [14] as

$$\tau_f=\epsilon\frac{m}{\sigma_a}\frac{1}{\rho_g v_m}, \tag{4}$$

where σ_a is the geometrical cross section of the particle, ρ_g is the gas density, v_m is the mean thermal velocity of the gas molecules, and ϵ is a numerical factor that is $\epsilon=0.58$. Equation (4) is valid for single grains as well as for dust aggregates. Therefore, the subsequent analysis is applicable even if the fragmentation process is incomplete in the sense that not only simple solid grains but also small aggregate fragments occur. The equation of motion can be solved analytically in the case of the force in Eq. (3) as

$$y=[v_{reb}\cos(\alpha)+v_{imp}]\tau_f(1-e^{-t/\tau_f})-v_{imp}t, \tag{5}$$

where the gas-particle beam is in the $-y$ direction, v_{reb} is the rebound speed, and α is the rebound angle with respect to $+y$. To derive this equation $-[v_{reb}\cos(\alpha)+v_{imp}]$ has to be chosen as initial gas velocity with respect to the particle in Eq. (3). This results from adding up the motion of the gas downwards to the target and the motion of the rebounding particle upwards from the target. We also get

$$x=v_{reb}\sin(\alpha)\tau_f(1-e^{-t/\tau_f}) \tag{6}$$

as position of the particle along the target edge as a function of time, t. In Eqs. (5) and (6) the particle position is given with respect to the impact point and t is measured from the time of impact. α can range as $-\pi/2<\alpha<\pi/2$. It should be noted that the last term on the right-hand side of Eq. (5) is due to the motion of the gas relative to the target that eventually brings a particle back to the target. Using Eqs. (5) and (6) the time scales to complete an arc of ≈ 100 μm in length and height would be several hundred μs at the given experimental parameters. Hence, we carried out additional experiments to image the tracks in the experiment. We set the pulse length of the laser to 0.5 ms that emphasizes the trajectory shapes rather than giving information on particle velocities (the pulse length was 10 μs before).

Because the dust beam during an injection is very dense, not surprisingly the images were oversaturated. However, at the time of the experiment, when the vacuum chamber is still

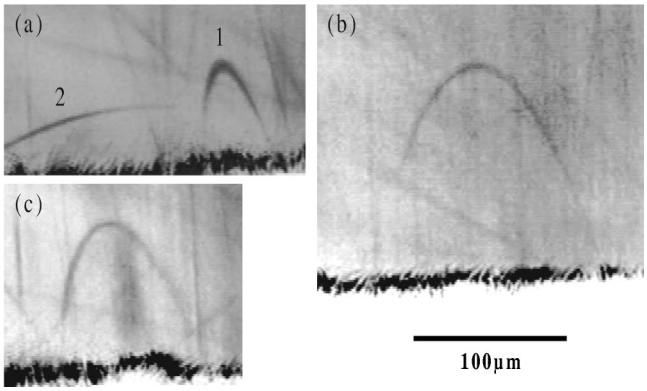

FIG. 4. Curved trajectories of particles heading back to the target. The curves are marked by letters and numbers for identification of the tracks in Fig. 5.

evacuated a less denser beam of aggregated particles leaves the TMP as mentioned above. For those aggregates, tracks of the rebounding particles could be imaged and indeed a large number of the expected arcs showed up. Examples are given in Fig. 4. In general, more tracks could be found on the images that are almost straight indicating high rebound velocities, but then the dust beam initially consists of a lot of single particles or dimers, which rebound at high velocities. It is also rather likely that the velocity distribution changes as soon as the target is covered with the first layers of dust particles, but there is not enough data to determine this in a reasonable way so far. Figure 5 shows the results of some calculations fitted to the measured particle tracks of Fig. 4 by means of Eqs. (5) and (6) that are in good agreement with the data. The gas velocity was set to the measured particle velocity determined in an earlier experiment with the same experiment parameters but with $t=10$ μs illumination time, being $v_{gas}=12$ m/s at a pressure $p=0.5$ mbar for a $d=127$ μm brass target. Coefficients of restitution varied between $c_r=0.057$ and 0.092 and rebound angles α with respect to the y axis ranged between $\alpha=12°$ and 55° for the calculations. The measured misalignment between the incoming particle (and gas) beam (y axis) and the image y axis of $\approx 3°$ was also taken into account. Actually, this small deviation from perfect alignment between the gas beam and the image y axis is responsible for most of the asymmetry that can be seen in the tracks of Fig. 4. There is also an intrinsic asymmetry in the tracks (which are not parabolic) but this is small.

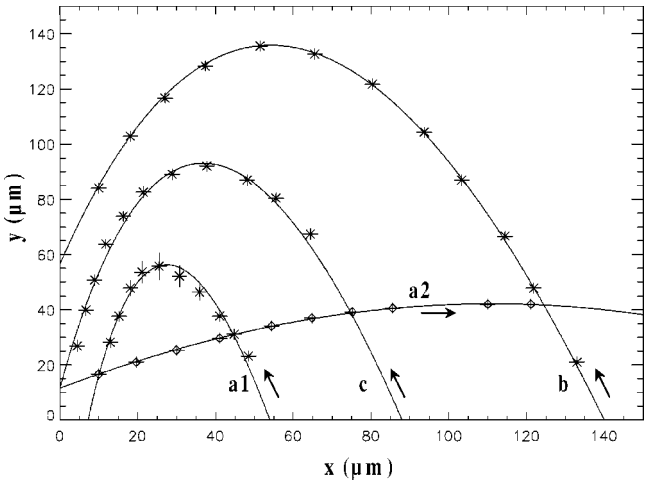

FIG. 5. Calculated trajectories fitted to particle tracks in Fig. 4 (identified by same letters and numbers as in Fig. 4). Due to the slight intrinsic asymmetry of the tracks, the heading of the particles can be inferred, which is indicated by the arrows.

Assuming a given gas velocity equal to the incoming particle velocity, the trajectories are determined unambiguously by one choice of rebound angle and rebound velocity. However, it has only been a reasonable assumption so far that gas and dust particles have the same velocity in the beam. Despite the fairly good coupling between dust and gas and the high dust density that should itself have a significant drag on the gas it cannot be *a priori* ruled out that the gas might relax more easily with the surrounding environment. The result would be a lower gas velocity compared to the particle beam. This would be important since it is the gas drag that eventually leads to sticking after fragmentation. There is no method implemented in the experiment to determine the gas velocity at the target apart from the particle velocity. However, this can be achieved by measuring the length of a track imaged during the whole time of illumination so that also the time of flight would be known. This would determine the mean particle velocity that in turn would lead to an unambiguous choice of rebound angle and gas velocity. Unfortunately, due to the small focal depth of the microscope of ≈ 80 μm, most tracks appear from or vanish into unfocused regions or are small arcs close to the target and therefore we could not find an arc that we could track for the whole illumination time of $t=500$ μs. Nevertheless, track b in Fig. 4 could be tracked over a significant time. Assuming the gas velocity to be the same as the dust particle velocity, the time of flight for the track would be $t=450$ μs. It should be noted that the track starts at its right end at the target (though hard to see in Fig. 4), but cannot be traced back further due to unfocused conditions and high speed of the precursor beam particle. So this is only a lower limit for the path length and it might be larger. Nevertheless, assuming the worst case that the laser beam was switched on the moment the particle bounced off the target and we imaged the whole track, the time of flight has to be $t=500$ μs. This can be achieved by decreasing the particle velocity by about 10% and in response to that also decreasing the gas velocity by 20% to fit the data again. This gives a lower limit to the gas velocity of 80% of the measured impact velocity. Within this error, the gas velocity would still be comparable to the impact velocity of dust grains in the beam.

A reduced gas velocity would even increase the importance of the measured effect. In this context it might be noticed that there seems to remain a small systematic deviation between most tracks and the fitted curves in Fig. 5, reaching close to the error margin, that was taken to be the thickness of the track. Within the before-mentioned possible small deviations between grain and gas velocity, there might also be a slight deviation in their directions. The fit in Fig. 5 used the measured angle of 3° between grain beam and image y axis,

and we regard the match as sufficient. Nevertheless, assuming only a few degrees deviation would make the fits almost perfect.

A. Comparison to possible effects of similar outcome

To rule out any doubts about the nature of the effect, we next consider if other effects could have played a role in the experiments.

• Gravity: The experiments were performed under normal laboratory conditions. Therefore all particles are subject to the gravitational force $F=mg$, with $g=9.8$ m/s^2, which eventually will lead to a settling of all suspended particles on the bottom of the vacuum chamber. To estimate the magnitude of the effect, the acceleration g has to be compared to v/τ_f as given in Eq. (3). For the 1.2 μm SiO_2 particles used in the experiments at a minimum pressure of 0.5 mbar of standard air, $\tau_f=3.2$ ms [Eq. (4)]. The smallest threshold velocity for sticking (Fig. 3) is $v\approx 6$ m/s and, hence, the smallest value for $v/\tau=1875$ m/s^2. This is more than two orders of magnitude larger than g. Gravity is therefore negligible for the experiments. However, if the effect on larger bodies will be studied in the future, where necessarily pressures have to be decreased and gas-grain coupling times of larger or more compact fragments might be higher, microgravity environments will be necessary.

• Electrical charge: Poppe *et al.* [15] found the possibility of collisional charging of insulating targets and single dust particles at collision velocities of several m/s that could lead to trajectories returning to the target again. We do not exclude the fact that particles could also have been charged in the experiments discussed here. However, the targets were grounded metal targets, and the whole setup was within a metal chamber. Due to the large windows it is not impossible that electric fields could exist within the chamber, but it is unrealistic that they would reach the required strength to influence a charged particle pulling it back to the target. In addition, most particles of an aggregate will never have contact with the actual target but will break contact between themselves and particles in the dust layers on the target. Therefore, both signs of charge should be present and visible as repelled or attracted trajectories if the electrical field would be strong enough. This is in contrast to the fact that only tracks bound to the target could be found. Furthermore, it is very unlikely that the fine-tuning of electrical field and charges would be such that the effect matches the gas drag, because if the effect would be too large, the measured pressure dependence of the critical sticking velocity should not be notable compared to a large pressure independent collisional charging. A similar fine tuning would be necessary to match the shape of the tracks, which can be fitted to a good extent under the assumption of gas drag as seen above but would in general look different under the influence of an electric field. We conclude that there is no evidence for (but rather against) electrical effects and that they have no significant effect on the outcome of the experiments.

• Incoming-outgoing collisions: The incoming particle beam is very dense. Estimates for the particle density based on a rough count of particles on the images [e.g., Fig. 2(b)] are on the order of $n=10^{13}$ m^{-3}. Taking the impact velocity as relative velocity v_{rel} in the order of $v_{rel}=10$ m/s and the collisional cross section $\sigma\approx 5\times 10^{-12}$ m^2, the collision time scale is $t=(nv_{rel}\sigma)^{-1}=0.002$ s. Therefore an average rebound particle will be hit every 2 ms. Assuming the case of a low coefficient of restitution $c_r=0.01$ the drag of the gas flow usually returns the particles to the target within a few hundred microsecond, which is considerably shorter than the collision time scale. Faster rebound particles with higher but still small coefficients of restitution $c_r=0.1$, however, might have traveled a significant distance $x\approx(1$ m/s$)(0.002$ s$)=2$ mm. Those particles will move far away from the impact area. They might leave the dense part of the beam altogether and will not necessarily collide with a beam particle. If they do collide it is very unlikely that the collisions would redirect a significant number of particles back to the target (i.e., where the dense beam intersects the target and maximum growth is observed). For those reasons, though several midair collisions have been observed, these kinds of collisions are negligible for the overall effect of particle growth on the target.

B. Model predictions

We conclude that the observed growth of a particle layer atop the target edge is inevitably and exclusively caused by gas drag acting on low velocity fragments. However, the experiments do not offer an explanation for the detailed shape of the data curve shown in Fig. 3. Therefore, we next consider two models to explain the dependence of v_{stick} on S.

1. Constant coefficient of restitution model

The first model assumes that any fragment or ejected particle is characterized by one coefficient of restitution and one rebound angle. With this assumption we determine the scale parameter by calculating the width of a particle track starting and ending on a target and relating it to a fixed pressure for varying impact velocities. As can be seen in the match of the dash-dotted lines in Fig. 3 the value of the pressure is of no significant importance in the outcome of the scale parameter. This justifies the use of only one parameter—the scale parameter S. There is no distinguishable effect of increasing the target width versus increasing the pressure. By choosing a special rebound angle and coefficient of restitution the model curve can be moved around in the diagram. We arbitrarily chose $\alpha=45°$ and $c_r=0.03$ to equal the low velocity end of the data extrapolation. However, the slope of the curve is independent of the position in the diagram.

The model gives a much steeper rise than the data suggest. The significant deviation from such a simple model can be understood in terms of different effects. Since an efficient growth of the dust pile on the target only takes place if more particle fragments return and stick to it than particles are removed from the uppermost layer(s) by the impact and are lost, it might well be that higher impact velocities free more target particles and therefore more have to stick for growth to occur. This naturally leads to a flatter functional dependence of the critical sticking velocity on S. Another explanation for

a flatter rise to lower scale parameters might be a transition from a more molecular type of gas flow to a hydrodynamical gas flow. In the latter case the force F on a particle would not always be perpendicular and in the direction of the target, but streamlines in the vicinity of the target would rather be along the edge and particles could more easily be carried around the target. Going from very large to very small target sizes the flow will inevitably switch between the two limiting cases but it is difficult to predict what happens in between. The flatter slope might be attributed to the beginning of a shift in flow regimes. It might also be considered that the target edge is virtually infinite in length. This will certainly have an influence on the number of rebound particles that might hit the target while they are lost if the target would be circular with diameter d. The images show an increased rate of growth in the center of the beam, which makes it unlikely that the growth is generated significantly (or only) by particles with long trajectories. Nevertheless, on the scales given the unlimited extension of the edge could favor growth at large scale parameters. This would also flatten the curve.

2. Velocity distribution model

The experimental data are in agreement with a fairly simple fit for the threshold velocity for sticking,

$$v_{stick} = -(5.5\ \text{m/s})\ln(S) + 9.35\ \text{m/s}. \tag{7}$$

Though it cannot be explained by the constant coefficient of restitution model described above, reasonable assumptions lead to the measured dependence. Until more detailed measurements are developed, the following might serve as a crude model to describe the impacts of aggregates embedded in a gas flow.

Below the observed threshold velocities, where a net growth on the target occurs, the gain of mass of this growing dust pile on the target by sticking of particles from the impinging aggregates must be larger than the loss of particles ejected from the dust layer during the impact. Since the monomers created in the collision leave the target with a certain distribution of velocities, a certain number of monomers has to be slow enough to return to the target. The equilibrium between gain and loss of mass might be expressed as

$$\int_0^{v_{crit}} \frac{dN_{aggregate}}{dv} dv = \int_{v_{crit}}^{\infty} \frac{dN_{ejecta}}{dv} dv. \tag{8}$$

Here, dN/dv are the velocity distributions for the fragments (monomers) of the incoming aggregate (indexed by aggregate) and of the ejected particles from the target dust layer (indexed by ejecta). The left-hand side of Eq. (8) describes the gain of particles by the fraction of monomers that are slow enough to be captured in a secondary collision, therefore describing the growth. The right-hand side of Eq. (8) describes the fraction of monomers that is ejected from the uppermost dust layers of the target and is fast enough to pass the target and thus is lost from the dust pile. This term characterizes the erosion. There is a critical velocity v_{crit} that determines the possibility for a monomer to return and stick to the target or to be too fast and pass the target. We consider here a value for v_{crit} averaged over all possible rebound angles or flight directions and impact locations on the target. This threshold rebound velocity for a monomer to stick should not be confused with the threshold impact velocity for the whole aggregate as actually observed in the experiments, v_{stick}, defined by a net growth.

We now assume a power law with two cutoffs for the velocity distributions, the same for both distributions. We regard this as a reasonable assumption to start with. A power law with two cutoffs is suggested by collisions of a grain on a granular bed as reported by Rioual *et al.* [16]. The slope they find is close to -2, but then the physics of micron-sized particles is different from that of millimeter particles that they used. Since we qualitatively find a lot of particles at higher rebound velocities, we take a slope of -1 to account for this. It should be noted that, in principle, the velocity distribution can be measured from particle tracks in our experiments. This is a more complicated task though and requires a statistically large sample, calculations for each track to the original rebound parameters, and a model to correct the two-dimensional projections to three-dimensional tracks. The limited focal depth might add additional selection effects that have to be considered carefully. Such an analysis will be a core requirement in understanding the collisions in more detail and in verifying the model given here. However, it is beyond the scope of this paper. Therefore we take here

$$\frac{dN}{dv} = N_c v^{-1} \quad v_{small} < v < v_{large},$$

$$\frac{dN}{dv} = 0 \quad v < v_{small}, \quad v > v_{large}. \tag{9}$$

Equation (8) can then be expressed as

$$\int_{v_{small}}^{v_{crit}} \frac{N_{agg}}{v} dv = \int_{v_{crit}}^{v_{large}} \frac{N_{eject}}{v} dv, \tag{10}$$

with N_{agg} and N_{eject} scaling the number of ejecta to the number of particles in an aggregate. Integration results in

$$N_{agg} \ln(v)\big|_{v_{small}}^{v_{crit}} = N_{eject} \ln(v)\big|_{v_{crit}}^{v_{large}}. \tag{11}$$

We will now derive an expression for the critical velocity v_{crit}. Typical values for the coefficient of restitution $c_r = v_{reb}/v_{imp}$ of particles that can return to the target are below $c_r = 0.1$. This can be seen from the calculations fitted to the measured tracks in Fig. 5. For such small ratios and for rebounds that are not too close to horizontal or vertical directions, the jump time of a particle on the target can be approximated by

$$t_{jump} = \frac{v_{reb} \tau_f}{v_{imp} \sin(\alpha)}, \tag{12}$$

as a comparison with numerical calculations of the jump time using Eq. (5) shows. Therefore with Eq. (6) the jump length would be

$$x_{jump} = v \sin(\alpha)\tau_f \left(1 - \exp\left[\frac{-v}{v_{imp}\sin(\alpha)}\right]\right). \quad (13)$$

To introduce the scale parameter we first note that the gas grain coupling time is proportional to the mean free path of the gas molecules. This can be deduced from Eq. (4) since the mean free path is inversely proportional to the gas density. Thus Eq. (4) can be written as

$$\tau_f = \frac{\lambda}{v_f}, \quad (14)$$

where v_f is defined by λ/τ_f resulting from Eq. (4). At the critical velocity $v = v_{crit}$ we set $x_{jump} = d/2$, since a particle starting in the center of the target edge will return to the target before it can reach the end of the edge and we regard $d/2 = x_{jump}$ as a suitable approximation on average including particles starting at different locations. Substituting v and x_{jump} by v_{crit} and $d/2$ in Eq. (13), and using Eq. (14) in Eq. (13), d and λ are introduced in the equation and can further be substituted by the definition of the scale parameter as given in Eq. (2). The result is

$$\frac{1}{2S} = v_{crit}\frac{\sin(\alpha)}{v_f}\left(1 - \exp\left[\frac{-v_{crit}}{v_{imp}\sin(\alpha)}\right]\right). \quad (15)$$

It has already been assumed that v_{reb}/v_{imp} is not too large (0.1). If in addition $\alpha > 10°$, the exponential function $[1 - \exp(x)]$ can be expanded and approximated by the linear term within an accuracy of 30% (15% for $\alpha > 20°$). Since we could not see a preferred rebound angle so far this approximation will be reasonable for most of the particles.

$$\frac{1}{2S} = v_{crit}^2 \frac{1}{v_f v_{imp}} \quad (16)$$

or

$$v_{crit} = \sqrt{v_{imp} v_f \frac{1}{2S}}. \quad (17)$$

Inserting this in Eq. (11) and performing some algebraic transformations results in

$$\frac{N_{agg}}{(N_{agg}+N_{eject})}\ln\left(\frac{v_{imp}v_f}{2v_{small}^2}\right) + \frac{N_{eject}}{(N_{agg}+N_{eject})}\ln\left(\frac{v_{imp}v_f}{2v_{large}^2}\right) = \ln(S). \quad (18)$$

We now further assume that the ratio of the number of ejecta to aggregate fragments is (much) smaller than 1. This has to be true at impact velocities only slightly higher than the fragmentation limit for an aggregate because the dust layer on the target is much more compact. This means that on average more bonds have to be broken to free a particle in the target than have to be broken in the fractal impacting aggregates. Since more energy is dissipated by this, it is likely that initially less particles are ejected than are generated by the aggregate destruction. Therefore, we assume for all given impact velocities that

$$N_{eject} \ll N_{agg}. \quad (19)$$

As it must be true for the low collision velocities, this assumption also certainly breaks down at very high impact velocities where already a single impacting particle will eject several particles from the target. However, this simplifies Eq. (18) to

$$\ln\left(\frac{v_{imp}v_f}{2v_{small}^2}\right) + \frac{N_{eject}}{N_{agg}}\ln\left(\frac{v_{imp}v_f}{2v_{large}^2}\right) = \ln(S). \quad (20)$$

Keeping in mind that a significant amount of energy might be dissipated by the fragmentation, we assume energy conservation in the sense that if v would be a typical velocity of an ejected particle,

$$v_{imp}^2 \propto N_{eject} v^2, \quad (21)$$

where v might be set to be the cutoff parameters v_{small} or v_{large}. Though carried out with much larger particles, the experiments by Rioual *et al.* [16] further suggest that the total number of ejecta scales linearly with the impact velocity that defines a proportionality constant v_{ej},

$$v_{ej} := \frac{v_{imp}}{N_{eject}}, \quad (22)$$

which would leave Eq. (21) to be

$$v = \sqrt{v_{imp} v_{const}}. \quad (23)$$

Following this line of reasoning, we assume

$$v_{large} = \sqrt{v_{imp} v_{lg}}, \quad v_{small} = \sqrt{v_{imp} v_{sm}}, \quad (24)$$

where v_{lg} and v_{sm} are assumed to be constant for each cutoff parameter. Inserted in Eq. (20) the result is

$$\ln\left(\frac{v_f}{2v_{sm}}\right) + \frac{v_{imp}}{v_{ej}N_{agg}}\ln\left(\frac{v_f}{2v_{lg}}\right) = \ln(S) \quad (25)$$

or

$$v_{imp} = \frac{1}{\ln\left(\frac{v_f}{2v_{lg}}\right)} N_{agg} v_{ej} \ln(S) - \frac{1}{\ln\left(\frac{v_f}{2v_{lg}}\right)} N_{agg} v_{ej} \ln\left(\frac{v_f}{2v_{sm}}\right) \quad (26)$$

or

$$v_{imp} = a \ln(S) + b, \quad (27)$$

where the constants a and b contain the various model parameters. We will now estimate absolute values for the constants a and b based on the experimental parameters.

Determining a: v_f is 0.04 m/s that can be calculated by Eqs. (4) and (14) (e.g., $\tau_f = 3.2$ ms, $\lambda = 132$ μm at p

$=0.5$ mbar or $\rho_g = 6.0 \times 10^{-4}$ kg m^{-3}). v_{large} might be of the order of the impact velocities, since such tracks are seen in the data (see, e.g., Fig. 2). Thus, in this case $v_{large} \approx 10$ m/s, which gives $v_{lg} = 10$ m/s and therefore $\ln[v_f/(2v_{lg})] = -6.2$. For the approximation in Eq. (19) the ratio N_{agg}/N_{eject} has to be $N_{agg}/N_{eject} \gg 1$ and assuming the limit to be as low as $N_{agg}/N_{eject} = 3.5$ thus yields $N_{agg} v_{ej} \approx 35$ m/s. The final result is $a = -5.6$ m/s.

Determining b: The cutoff for the smallest velocity is at least smaller than a few percent of the impact velocity, since a number of coefficients of restitution of this order is observed. We choose 2% as a cutoff or $v_{small} = 0.2$ m/s that gives $v_{sm} = 0.004$ m/s. This in turn gives $\ln[v_f/(2v_{sm})] = 1.61$. Multiplied with $-a$ finally results in $b = 9.0$ m/s.

The model thus results in

$$v_{imp} = -5.6 \text{ (m/s)} \ln(S) + 9.0 \text{ m/s}, \tag{28}$$

which can be compared to the result found as a log-linear fit to the experimental data given as Eq. (7).

Within the broad model assumptions this is sufficient quantitative agreement between model and data to support the principal idea behind the experiment. It has to be noted that some of the assumptions were chosen to fit the data, and actually fine tuning the assumptions beyond the rough estimates above would allow a perfect fit. With respect to these partly arbitrary choices, the proposed model is not necessarily describing the underlying physics of these collisions in detail. It is our intention to describe at least one physical way to explain the dependence of the threshold velocity for sticking on the scale parameter. The model is thus a working hypothesis until more data are obtained to verify or refine the assumptions.

IV. APPLICATIONS AND OUTLOOK

We performed the experiments with protoplanetary growth in mind, and it is clear that the effect found might be a very important process to provide efficient growth of larger objects. However, we feel that the results might also be important for other basic scientific or applied branches besides astrophysics, where sticking of dust particles is of any concern. The results might be of importance for industrial application, where dust powders are processed, since it clearly shows a difference in sticking behavior between single dust particles and assemblies of dust particles, which might easily occur in dense particle clouds. Here, considerations about gas flows might be essential. It might lead to an effective way to separate different sizes of particles (or just big ones from the rest) if other ways (e.g., by sifting) are not applicable since the sticking depends on the coupling time of the particles, but those are merely our speculations so far.

Since the experiments performed here only refer to (small) CCA aggregates a scaling to centimeter or meter bodies is not possible in detail yet. To the knowledge of the authors there are no experiments that study such impacts with dust projectiles in the centimeter to meter size regime. However, besides the need to perform the basic experiments with dust projectiles, fragmentation seems a very likely process to take place in higher low speed collisions of larger compound bodies. In that case the results of this paper allow partly fragmented bodies to accumulate mass simply by having the gas driving the fragments to a larger body. The experiments are not yet sophisticated enough to predict the mean growth efficiency in a given collision but the effect discussed here might well turn out to be a major mechanism to overcome collisional disruption and turn it into fragmentational growth.

ACKNOWLEDGMENTS

We would like to thank the DFG for supporting G.W. J.B. is supported by the German Space Agency DLR. J.E. was supported by the NASA Microgravity Fluid Physics Program.

[1] G. Wurm and J. Blum, Icarus **132**, 125 (1998).
[2] J. Blum and G. Wurm, Icarus **143**, 138 (2000).
[3] S. J. Weidenschilling and J. N. Cuzzi, in *Protostars and Planets III*, edited by E. H. Levy and J. I. Lunine (University of Arizona, Tucson, 1993).
[4] T. Poppe, J. Blum, and Th. Henning, Astrophys. J. **533**, 454 (2000).
[5] C. Dominik and A. G. G. M. Tielens, Astrophys. J. **480**, 647 (1997).
[6] L.-O. Heim, J. Blum, M. Preuss, and H.-J. Butt, Phys. Rev. Lett. **83**, 3328 (1999).
[7] J. Blum and M. Münch, Icarus **106**, 151 (1993).
[8] K. D. Supulver, F. G. Bridges, S. Tiscareno, and J. Lievore, Icarus **129**, 539 (1997).
[9] J. E. Colwell and M. Taylor, Icarus **138**, 241 (1999).
[10] G. Wurm, Ph.D. thesis, Friedrich-Schiller Universität, 1997.
[11] G. Wurm, J. Blum, and J. E. Colwell, Icarus **151**, 138 (2001).
[12] J. A. Wood, Space Sci. Rev. **92**, 87 (2000).
[13] J. Blum, M. Schnaiter, G. Wurm, and M. Rott, Rev. Sci. Instrum. **67**, 589 (1996).
[14] J. Blum, G. Wurm, S. Kempf, and Th. Henning, Icarus **124**, 441 (1996).
[15] T. Poppe, J. Blum, and Th. Henning, Astrophys. J. **533**, 472 (2000).
[16] F. Rioual, A. Valance, and D. Bideau, Phys. Rev. E **62**, 2450 (2000).